Catalysis Letters (2022) 152:227–238
https://doi.org/10.1007/s10562-021-03620-w

Influence of Active Metal Precursors on the Structure and Catalytic Behavior of Pd/Al_2O_3 Catalysts for Selective Acetylene Hydrogenation

Tianxing Yang[1] · Min Zhao[1] · Xue Wang[1] · Rui Ma[2] · Yanan Liu[1,3] · Yufei He[1,3] · Dianqing Li[1,3]

Received: 14 January 2021 / Accepted: 4 April 2021 / Published online: 18 April 2021

Abstract

Choosing an appropriate metal precursor is a basic step in the preparation of catalysts. In this paper, $PdCl_4^{2-}$, $PdSO_4$ and $Pd(acac)_2$ were selected as the metal precursor, which was supported on α-Al_2O_3 commonly used in industry to explore the impact of palladium precursor on the structure and catalytic behavior for selective acetylene hydrogenation. The activity for the three catalysts is similar, while the ethylene selectivity of $Pd(acac)_2$ can outclass the other two catalysts at the fixed conversion. The different catalytic performance is mainly ascribed to the influence of non-metal residua distribution on valence state structure and size effect determined by HRTEM, CO chemisorption, XPS and in situ CO-IR. More importantly, the catalyst prepared by $Pd(acac)_2$ perform better stability due to the formation of the Pd carbide species after 24 h reaction. The catalytic deactivation with time-on-stream for other two catalysts was attributed to the sintering of Pd particles and carbon deposition under reaction conditions.

Graphic Abstract

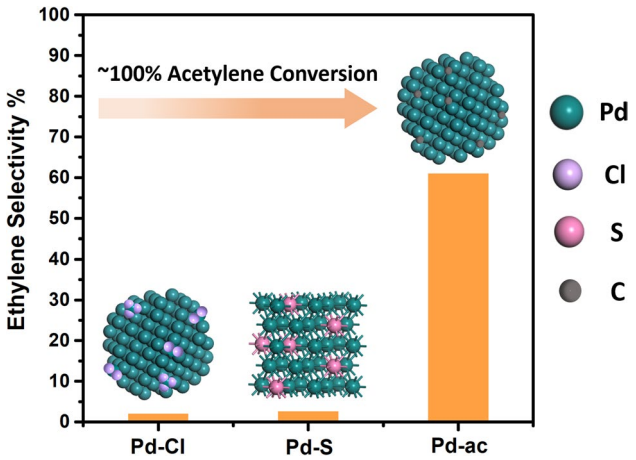

Keywords Palladium precursor · Selective acetylene hydrogenation · Non-metal residua · Valence state structure · Size effect

✉ Rui Ma
marui1840@163.com

✉ Yanan Liu
ynliu@mail.buct.edu.cn

✉ Yufei He
yfhe@mail.buct.edu.cn

Extended author information available on the last page of the article

1 Introduction

Supported metal catalysts is significantly important, possessing a wide range of applications in the petroleum refining and petrochemical industry. The nature of the metal precursor used in the catalyst preparation has a great effect on the properties of catalysts [1–3]. The metal chlorides are

commonly used as precursors for catalyst synthesis; however, the presence of chloride can promote polymerization of metal particles (for example gold) and suppress the activity of the catalysts [4]. In order to clear away chlorine, alternatively different washing methods for catalysts loaded with metal chloride precursors were utilized [5]. Meanwhile, metal ammonium nitrate, metal acetylacetonate, and other metal precursors have been also applied to avoid the chlorine [6, 7]. Li et al. prepared highly dispersed Pd/SiO_2 catalysts by impregnating SiO_2 with $Pd(acac)_2$, which exhibited superior performance against sintering at high temperature in partial oxidation of methane reaction [8]. Mahata et al. synthesized Pd/Al_2O_3 and Pd/MgO catalysts from $Pd(NH_3)_4Cl_2$, $PdCl_2$ and $Pd(CH_3COO)_2$ precursors, finding that the absence of residual chlorine in the Pd particles offers better dispersion [4]. $Pd(NH_3)_4Cl_2$ leads to lower dispersion than $PdCl_2$ probably due to the presence of inherent NH_3 (a reducing agent) and facile surface mobility of the precursor. However, other studies reported that the use of $PdCl_2$ instead of $Pd(NO_3)_2$ or $Pd(OOCCH_3)_2$-based salts as a noble metal precursor on silica supported was more dispersed and showed better catalytic activity for an oxidation of hydrogenation [9]. Followed by these, Marceau et al. found that $Pt/\delta\text{-}Al_2O_3$ catalysts using H_2PtCl_6 precursor exhibited an inhibiting effect on the activity toward methane oxidation owing to chloride ions located on the metal-support interface [10]. Based on these report, it's wildly accepted that the metal precursor plays an important role on the structure of catalysts, which usually make a difference to catalytic performance.

Selective hydrogenation of acetylene is a significant reaction for petrochemical industry, which plays a decisive role in the development of national economy. Supported Pd-based catalysts are one of the most effective methods to achieve this selective hydrogenation process [11]. In terms of palladium, the adsorption energy of acetylene on Pd (111) atop sites is − 13.1 kcal/mol, much higher than that of ethylene (− 7.0 kcal/mol), which means Pd catalysts favour the adsorption of acetylene but limit ethylene. Even so, ethylene is readily hydrogenated to ethane with the decrease of the content of acetylene. Therefore, it is crucial to develop more efficient catalysts for this reaction by tailoring the properties of Pd-based catalysts. In recent years, it has been an emerging way to regulate the properties of the Pd active component by controlling the diverse coordination environment of the Pd atoms, so as to obtain the excellent catalytic performances. The most common method is to introduce a second metal to obtain bimetallic catalysts, such as PdAg [12–14], PdCu [15–17], PdZn [18, 19], PdGa [20, 21], PdCo [22], etc., which show better ethylene selectivity than monometallic Pd catalyst. Regulating the metal-support interaction has also been widely concerned. For example, He reported the Pd/LDO catalyst possessed better activity and ethylene selectivity than Pd/Al_2O_3 and Pd/MgO, which was attributed to higher dispersion and decreasing electronic density of Pd originating from the interaction between Pd and acid sites on LDO support [23]. However, the exact influence of the palladium precursor used during the catalyst preparation on the local atomic and electronic structure of Pd active site and catalytic behavior in acetylene selective hydrogenation are rarely explored. Moreover, a fragment of precursor as residual, such as Cl or S often naturally present in hydrocarbon feedstocks, may be attached to the active component and thus result in deactivation.

In this paper, $Pd/\alpha\text{-}Al_2O_3$ catalysts were prepared using $PdCl_4^{2-}$, $PdSO_4$, and $Pd(acac)_2$ as metal precursors by using simple impregnation method. Powder X-ray diffraction (XRD) and high-resolution transmission electron microscope (HRTEM) were employed to investigate the crystal structure and size of Pd particles. The metal loading of samples was determined by inductively coupled plasma atomic emission spectrometer (ICP-AES), and the contents of precursor residual were determined by X-ray fluorescence (XRF) measurement. The status and electronic environment of surface Pd atoms were revealed by in situ diffuse reflectance infrared fourier transform spectroscopy (CO-IR) and X-ray photoelectron spectroscope (XPS) analysis. Moreover, the characteristics of the ethylene adsorption on Pd sites were shown by C_2H_4-IR and temperature-programmed desorption (TPD). The catalytic performance and the deactivation mechanism of Pd/Al_2O_3 catalysts that prepared from different metal precursors in the selective hydrogenation of acetylene was investigated in a fixed bed reactor.

2 Experiment

2.1 Catalyst Preparation

Pd/Al_2O_3 catalysts were prepared using Na_2PdCl_4, $PdSO_4$ (Sino-Platinum Metals Co. Ltd., China) and $Pd(acac)_2$ (34.7% wt% Pd, Alfa Aesar) as metal precursors, employing the marginally excess volume wetness impregnation method under vigorous stirring at 80 °C. In detail, about 2 g of Al_2O_3 (≥ 99%, Aldrich, $S_{BET} = 14\ m^2 \cdot g^{-1}$, heat-treated in air at 1200 °C for 3 h) was added to the calculated amount of metal precursor solutions (1% theoretical Pd loading). $Pd(acac)_2$ was dissolved in chloroform, while Na_2PdCl_4 and $PdSO_4$ were used as an aqueous solution. After solvent was removed by evaporation, the residues were dried overnight at 110 °C in an air oven. The catalysts were subsequently calcined in 10% H_2/N_2 at 400 °C for 4 h to produce metallic Pd nanoparticles on the support. Pd/Al_2O_3 catalysts obtained from Na_2PdCl_4, $PdSO_4$, and $Pd(acac)_2$ were denoted as Pd-Cl, Pd-S and Pd-ac, respectively.

2.2 Characterization

Schimadzu ICPS-7500 inductively coupled plasma atomic emission spectrometer (ICP-AES) and a PANalytical Axios Advanced wavelength dispersive X-ray fluorescence (WDXRF) spectrometer were used to record elemental content, including palladium, sulfur and chlorine. The carbon content was analysed by Vario EL cube organic element analyzer. The morphology, particle size and lattice fringes of the samples were examined using a JEOL JEM-2100F high-resolution transmission electron microscopy (HRTEM). Powder X-ray diffractions (XRD) of the samples were obtained using a Rigaku Miniflex powder X-ray diffractometer equipped with a Cu K_α radiation source ($\lambda = 0.15418$ nm) by applying a scanning rate of 1.2 degree per minute in the 2θ range of 10°-70°. X-ray photoelectron spectroscopy (XPS) was conducted on an Axis Supra spectrometer (Kratos, Japan) using Al K_α radiation (1486.6 eV). The binding energy of samples was calibrated using the binding energy of the C 1 s peak (284.6 eV) as a reference. In situ Fourier-transformed infrared absorption spectroscopy of CO and C_2H_4 experiments was performed on Nicolet 380 instrument spectrophotometer at a spectra resolution of 4 cm^{-1}.

2.3 Selective Hydrogenation of Acetylene

Gas phase selective hydrogenation of acetylene was performed in a fixed-bed quartz micro-reactor with relative pressure of 0.4 MPa. 50 mg of the catalysts and 1.35 g quartz sand were mixed and loaded at the center of 7 mm quartz tube. 167.5 mL/min gas flow consisting of 33% C_2H_4/ 0.33% C_2H_2/ 0.66% H_2/ balance N_2 gave a space velocity (SV) of 10,056 h^{-1} and a H_2/C_2H_2 ratio of 2:1. The gas composition from the micro-reactor outlet was analysed by online gas chromatography equipped with a flame ionization detector online using PLOT capillary column (50 m × 0.53 mm). Prior to the reaction, the catalyst was pre-treated with H_2/N_2 at 150 °C for 1 h. In the reaction process, the carbon balance determined from the effluent gas was 100 ± 5%. Acetylene conversion, ethylene selectivity and TOF were calculated as follows:

$$C_2H_2 \text{ conversion} = \frac{C_2H_2(\text{inlet}) - C_2H_2\ (\text{outlet})}{C_2H_2\ (\text{inlet})}$$

$$C_2H_4 \text{ selectivity} = \frac{C_2H_4(\text{outlet}) - C_2H_4\ (\text{inlet})}{C_2H_2(\text{inlet}) - C_2H_2\ (\text{outlet})}$$

$$\text{TOF} = \frac{A}{n \times D} (A = \text{moles of acetylene conversion per second; n = Pd moles in the catalyst; D = metal dispersion})$$

Temperature programmed H_2 reduction (H_2-TPR), Temperature programmed H_2 and C_2H_4 desorption (H_2/C_2H_4-TPD) and CO chemisorption were performed on a Micrometric Chemisorb 2920. The catalysts precursor were pretreated at 120 for 30 min under Ar stream and then H_2-TPR was carried out with a heating rate of 10 °C/min in a stream of 10% H_2/ Ar from 50 to 400 °C. For the H_2/C_2H_4-TPD, the catalysts were pretreated at 120 °C for 30 min under 10% H_2/Ar and then cooled to room temperature. The catalysts were then kept in a flow of H_2 or C_2H_4 for 60 min to saturated adsorption. Physical absorption H_2 or C_2H_4 molecules were removed in the flow of Ar or He for another 30 min, and then the programmed desorption process was carried out from room temperature to 600 °C in the flow of Ar or He at a rate of 10 °C/min. The CO chemisorption pretreated condition was similar to the H_2/C_2H_4-TPD and then performed using a pulse (50 µL) titration procedure. 20 times pulse were conducted at room temperature until adsorption saturation. Thermal analysis was performed on a TG/ DTA X70 Thermogravimetric analyzer from 50 to 800 °C with a rate of 10 °C/min.

The Weisz-Prater and Mears criterion were employed for eliminating the effect of heat and mass transfer over Pd/Al_2O_3 catalyst (shown in supporting information and Table S1) [24, 25]. The results from Weisz-Prater criterion suggest the effect of external and internal diffusion could be ignored.

$$\frac{-r'_A \times \rho_b \times R \times n}{k_c \times C_{Ab}} = 2.1 \times 10^{-7} < 0.15$$

$$C_{WP} = \frac{-r'_A \rho_c R^2}{D_e \times C_{As}} = 2.5 \times 10^{-6} < 1$$

The result from Mears criterion indicates that the interphase and intra-particle heat transfer or mass transport have no effect on the reaction.

$$\frac{-r'_A \times R^2}{C_{Ab} \times D_e} < \frac{1 + 0.33\gamma\chi}{\left|n - \gamma_b \times \beta_b \times (1 + 0.33n \times \omega)\right|}$$

Table 1 Elements content in all the Pd/Al_2O_3 catalysts

Catalysts	Pd (wt%)[a]	Cl (wt%)[b]	S (wt%)[b]	C (wt%)[c]	Atomic ratio of Pd:Cl/S/C
Pd-Cl	0.93	0.46	–	–	1:1.5
Pd-S	0.89	–	0.21	–	1:0.8
Pd-ac	0.91	–	–	0.26	1:0.4

[a]Determined from ICP-AES

[b]Determined from XRF

[c]Determined from organic element analysis using a Vario EL cube

3 Results and Discussion

Three Pd/Al_2O_3 catalysts were prepared using different precursors. It is primary to determine the metal loading and the content of non-metal element. As listed in Table 1, the metal loading of samples determined by ICP-AES measurement is slightly lower than the nominal value (1%) but the value is reproducible. Furthermore, the precise content of chlorine and sulfur in Pd-Cl and Pd-S sample were determined by XRF measurement. The atomic ratio of Pd: Cl and Pd: S are smaller than the theoretical data (1: 2 and 1: 1 respectively). This decrease of Cl and S contents can be attributed to the formation of HCl and H_2S in the reduction process. The carbon residue of Pd-ac sample was analyzed by organic element analysis, which is much lower than the C content of $Pd(acac)_2$ precursor. The atomic ratio of Pd: C is 1: 0.4 while that is 1: 10 in $Pd(acac)_2$. The weight loss of C was ascribed to the decomposition of $Pd(acac)_2$ into CO_2 on the support surface at reduction process according to the literature [6]. The above results confirm that all the Pd catalysts surface

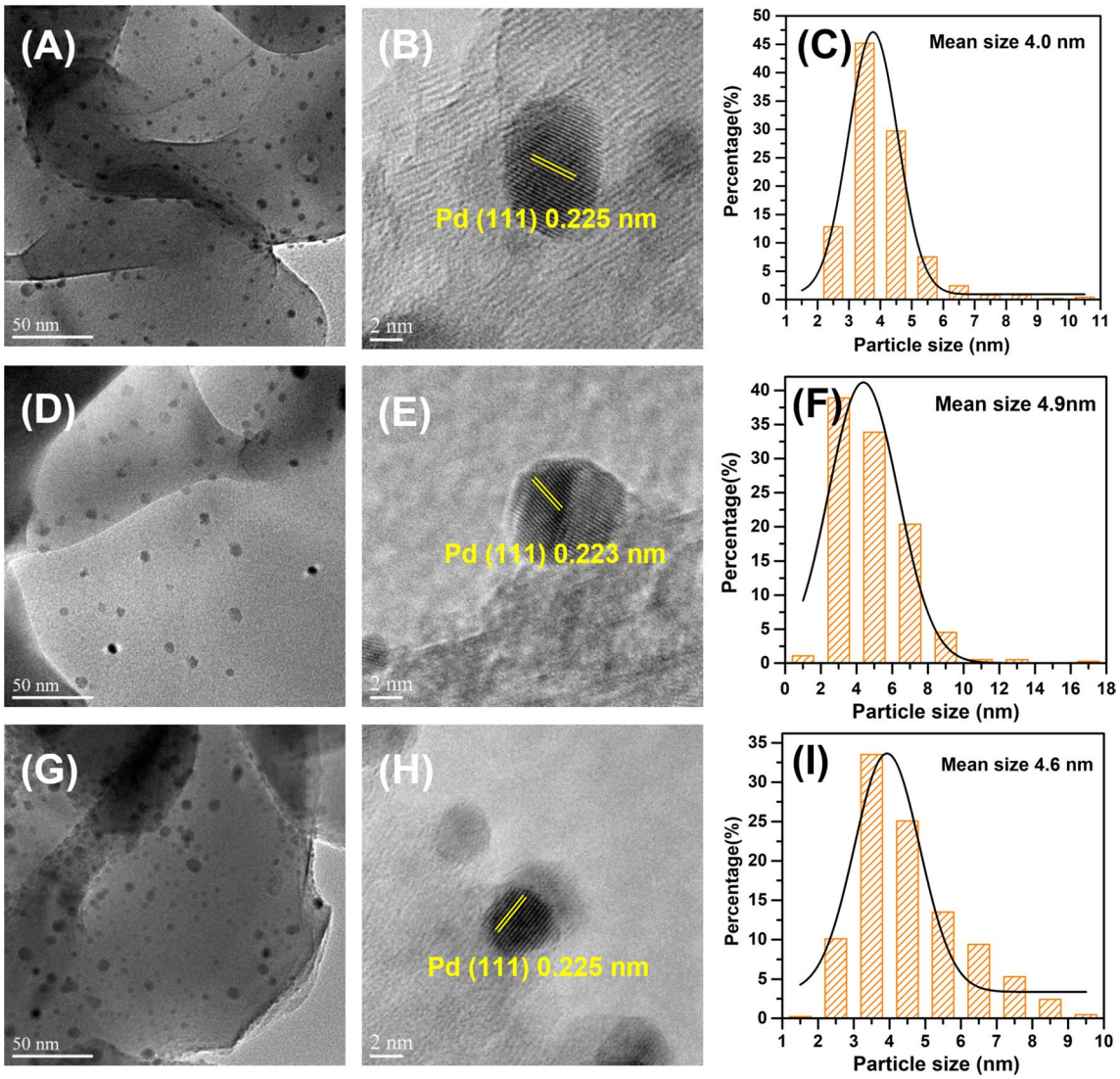

Fig. 1 HRTEM images and the corresponding size distributions of Pd catalysts over Pd-Cl (**a**–**c**), Pd-S (**d**–**f**), and Pd-ac catalysts (**g**–**i**)

contain some nonmetallic elements from the Pd precursor. Notably, chlorine residues are far more than that of sulfur and carbon.

To investigate the influence of the precursor residue species on the structure of as-prepared catalyst, representative TEM image of Pd nanoparticles and the associated particle size distribution are presented (Fig. 1). All metal particles exhibit a morphology of pseudo-sphere, indicating the metal precursors with different non-metal element residues show no effect on the morphology of active metals. However interestingly, the size of particles is influenced by the precursor ligands. Specifically, Pd-Cl sample presents a small size of 4.0 nm and the homogeneous distribution with > 80% particles in the size range of 1.5–4.5 nm, while the mean diameters of Pd-S and Pd-ac samples are 4.9 and 4.6 nm, respectively along with the wide size distribution. This is attributed to that chloride interacts with hydroxyl groups presented on the surface of alumina to form Pd oxychloride species ($Pd_xO_yCl_z$), contributing to a good metal dispersion. As shown in Table 1, Pd dispersion of Pd-Cl, Pd-S and Pd-ac determined by CO chemisorption are 25.9%, 21.9% and 22.2% respectively, which is consistent with HRTEM results. Further increasing TEM magnification, the lattice spacing of Pd nanoparticles could be observed. The Pd lattice fringe was detected to be 0.223 nm in Pd-S, which is slightly smaller than that of Pd (111) in Pd-Cl and Pd-ac samples (0.225 nm). The lattice compression for Pd-S sample may be due to the insertion of S to Pd lattice.

Moreover, powder XRD analysis was performed to explore the crystal structure. As showed in Fig. 2a, all samples exhibit the characteristic reflections of α-alumina (PDF#10-0173) suggesting that the metal precursor and impregnated solvent have little influence on the textural structure of the alumina support, which can also be proved by BET analysis (showed Table S2). The diffraction peak of Pd (111) at 2-theta of ca. 40° appears on all three Pd/Al_2O_3 samples. In details, the characteristic peak for Pd-ac catalyst is at 40.1° corresponding to the pure Pd metal (PDF#46–1043), which indicates that C residua did not get into the Pd nanoparticle lattice. In addition, the TG curve of fresh Pd-ac catalyst shows no weight loss peak of polymeric carbon (Figure S1). Based on the above analysis results, we consider that the slight C element mainly exists on the catalyst surface in the form of atomic carbon. Noted that this peak in Pd-S catalyst (40.3°) shifts to higher angle with respect to the corresponding peak position in Pd-ac. According to the literatures [26], sulfur atoms can insert the lattice of Pd and form palladium sulfide nanoparticles by thermal

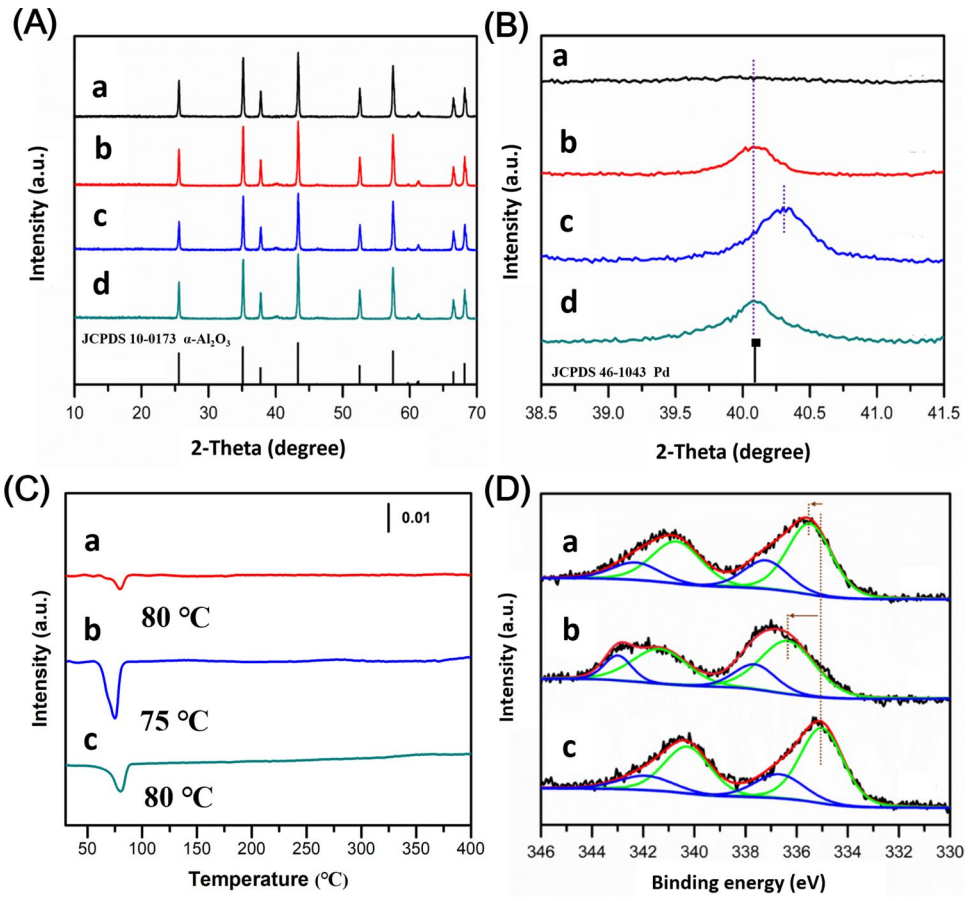

Fig. 2 **a**, **b** XRD patterns of the (a) Al_2O_3, (b) Pd-Cl, (c) Pd-S and (d) Pd-ac; **c** H_2-TPR profiles of Pd catalyst precursor (a) Pd-Cl, (b) Pd-S and (c) Pd-ac; **d** XPS spectra of (a) Pd-Cl, (b) Pd-S and (c) Pd-ac

treatment of $PdSO_4$ under H_2 atmosphere, which crystalline phase and element content depends on treated temperature. However, no obvious characteristic peak of sulfide is observed in Pd-S catalyst probably due to low sulfur content. As a result, the above shift is ascribed to the incorporation of sulfur atoms into Pd nanoparticle with a concomitant lattice contraction, which is in accordance with the HRTEM result. However, no obvious change of the characteristic peak position was observed in terms of Pd-Cl samples compared with Pd-ac, suggesting Cl elements does not enter the lattice. In order to further explore the existence form of Cl, UV–Visible results are shown in Figure S2. For the precursor of Pd-Cl sample, an absorbance band of around 285 nm was observed, which can be assigned to $PdCl_4^{2-}$ species [27, 28]. The result indicates that residual Cl still exist in the form of complexes with Pd. However, no obvious absorbance peak over Pd-Cl catalyst owing to the decrease of Cl content in the reduction process.

After confirming the existence form of different nonmetal element residues, we explored the influence of these element location on the reducibility and electronic structure of Pd metal by TPR and XPS analysis. H_2-TPR profiles of the different palladium precursors are shown in Fig. 2c. Only negative peaks at 75–80 ℃ is observed without reduction peak of each catalyst precursors due to the easy reduction of Pd species under hydrogen at low temperature. Monometallic Pd catalyst is easy to reacts with hydrogen to form PdH_x, which is thermally unstable and would decompose during thermal treatment to release H_2 [29, 30]. Therefore, the negative peaks could be attributed to the decomposition of PdH_x, which is commonly seen in supported Pd catalysts. Hydride composition, presented in Table 2 as H/Pd ratio. The order of H/Pd ratios for the three catalysts is Pd-Cl (0.19) < Pd-ac (0.21) < Pd-S (0.29). According to the report [31, 32], the formation of PdH_x is closely related to the size and structure of Pd particles, that is the H/Pd ratio declines with the decrease of the size of active components. The result is consistent with the Pd dispersion calculated by HRTEM and CO chemisorption.

XPS profiles for three representative catalysts (Pd-Cl, Pd-S, Pd-ac) are shown in Fig. 2d. The dominating XPS peak of Pd $3d_{5/2}$ with binding energy at 335.1 eV can be observed in Pd-ac samples, which is in good agreement with the value (335.2 ± 0.2 eV) reported by Briggs and Seah for Pd^0 [33]. The core level Pd $3d_{5/2}$ BE (336.8 eV) is assigned to Pd (II) species in PdO oxidized in air. Taking Pd-ac as a benchmark, Pd^0 on Pd-Cl and Pd-S catalysts exhibit a $Pd_{5/2}$ BE that is ~ 0.5 eV and ~ 1.2 eV higher than Pd-ac respectively. This phenomenon suggests the electron transfer from Pd to other species, resulting in the decrease of the electron density for Pd atom. Alvarez-Montero et al. reported a shift to higher BE for Pd/C that was attributed to electronic transfer associated with residual surface Cl [34]. Zhou et al. have also demonstrated the occurrence of electron-deficient Pd within 3.8–10.5 nm [35]. They linked this to the presence of surface species (e.g. HCl, SO_x and NO_x) generated during catalyst preparation that serve to modify the electron density of the Pd sites with formation of supported Pd^{n+} nanoparticles. Although the electronegativity of Cl (3.16) is stronger than that of S (2.58), the binding energy of Pd-S sample varies more. According to the literatures [26, 36], the formation of sulphide will lead to Pd atoms retaining a more positive charge, but due to low sulfur content this phenomenon is related to the introduction of S into the Pd lattice. Whereas Cl exists as Pd-Cl complex rather than the doping into Pd structure, which has lesser effect on the electronic structure of Pd. Additionally, as the shown in the Table S3, the presence of S and Cl also results in more Pd^{2+} than Pd-ac sample determined by integrating the XPS peak area.

The influence of precursor residues on geometric structure over the obtained catalysts was revealed by CO infrared spectroscopy analysis, which is an excellent method to probe the multi-adsorption geometries of metal nanoparticles. Figure 3 compares the FTIR spectra of CO over three Pd/Al_2O_3 catalysts obtained from different metal salt precursors. The

Table 2 The physicochemical properties of Pd/Al_2O_3 catalysts

Catalyst	Size (nm)[a]	Dispersion (%)[b]	CO uptake (μmol/g)[c]	Dispersion (%)[d]	H/Pd (mol mol^{-1})[e]	Pd $3d_{5/2}$ (eV)[f]
Pd-Cl	4.0	28.0	12.6	25.9	0.19	335.6
Pd-S	4.9	22.9	10.3	21.8	0.29	336.3
Pd-ac	4.6	24.3	9.5	22.2	0.21	335.1

[a]Determined by HRTEM

[b] $= \frac{6M_{Pd}}{\rho\sigma Ld}$ $(M_{Pd} = 106.42\,g/mol,\ \rho = 12.02 \times 10^6 gm^{-3}, \sigma = 0.79 \times 10^{-19} m^2, L = 6.02 \times 10^{23}, d:\ nanoparticlesize)$

[c]Determined by CO chemisorption

[d] $= \frac{\text{mol of CO adsorbed}}{\text{mol of metal}} \times (\text{linear CO fraction} \times 1 + \text{bridge CO fraction} \times 2)$

[e]Determined by H_2-TPR

[f]Recorded by XPS

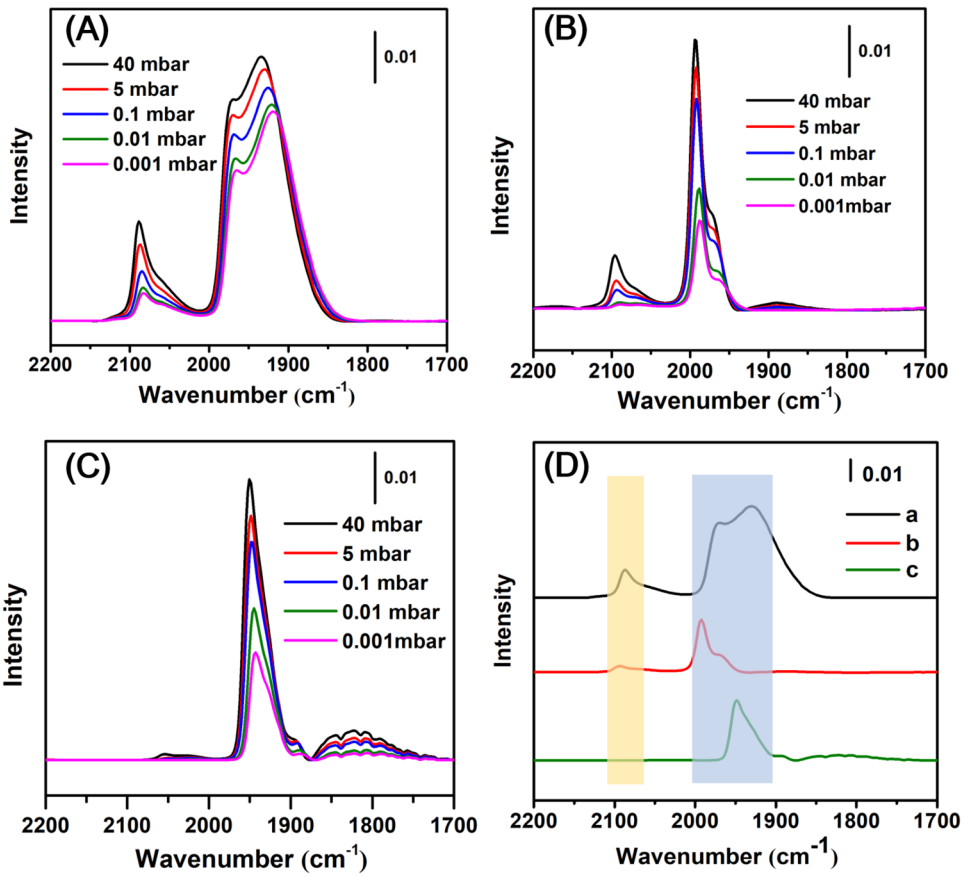

Fig. 3 In situ CO-IR spectra of **a** Pd-Cl, **b** Pd-S, **c** Pd-ac, and **d** three catalysts at 40 mbar (a) Pd-Cl, (b) Pd-S, and (c) Pd-ac

band between 2100 and 2000 cm^{-1} is due to linear adsorbed CO molecules on Pd defect sites such as kinks and corners, while multi-coordinated CO bands (various bridge-bonded species) locate between 2000 and 1800 cm^{-1} on Pd ensemble sites [37, 38]. CO is adsorbed by bridge-bond adsorption principally over the Pd-ac catalyst and almost no linear-bond CO adsorption was observed. The trace of C residua as atomic carbon on the catalyst surface has a limited influence on the dilution of adjacent Pd surface sites. Besides, the band at 1951 cm^{-1} over Pd-ac shifts to lower frequency on decreasing coverage indicating a degree of dipolar coupling for the CO residing in these site (bridge-bonded CO on particle) [38]. Notably, a new peak appears in the Pd-Cl catalyst at 2092 cm^{-1}, which can be attributed to CO adsorbed on low-coordinated Pd sites such as terrace and defect due to small Pd particle size. Two different bridge-bonded CO molecules can also be observed, in which the peak at 1969 cm^{-1} is assigned to bridge-bonded CO on Pd (100) facets and the peak at 1920 cm^{-1} is assigned to hollow- and bridge-bonded CO on Pd (111) planes. It is worthwhile noting that the linear CO state for Pd-S is unexpected to be populated to a significant degree (10.7%) (Table S3) under same conditions. Considering that the mean size of Pd-S samples is almost same as that of Pd-ac catalyst, the decrease of Pd ensemble sites suggests the fact that the addition of sulfur separates the contiguous Pd sites. In addition, as shown in Fig. 3d, the adsorption peak shift toward higher wavenumber in the following order of Pd-S > Pd-Cl > Pd-ac when the pressure is fixed at 40 mbar, which could be ascribed to the electronic effect. The shifts to higher wavenumbers indicate the electron density of Pd decrease [12], which is consistent with the XPS results.

The catalytic performance of this series of Pd/Al_2O_3 catalysts prepared from different palladium precursors in partial hydrogenation of acetylene was tested in a fixed-bed flow reactor. Figure 4a shows the plots of acetylene conversion versus temperature. With the temperature increasing, the conversion of acetylene increases over the three catalysts. In the fixed temperature range (30–60 ℃), the conversion of acetylene decreases in the order of Pd-Cl > Pd-S > Pd-ac catalysts. However, when the temperature reaches 62 ℃, acetylene conversion of Pd-S catalysts is fully consumed at first, while Pd-ac samples exhibits 100% conversion at 65 ℃, demonstrating the catalyst with $PdCl_2$ and $PdSO_4$ as Pd precursor are highly active relative to Pd-ac catalyst. Moreover, apparent activation energy values (E_a) for Pd catalysts with different precursor are obtained by plotting ln (TOF) versus 1/T [22], as shown in Fig. 4c. The E_a for acetylene hydrogenation over the Pd-Cl, Pd-S, and Pd-ac are 35.7, 49.1 and 55.7 kJ/mol, respectively. The significant decrease of

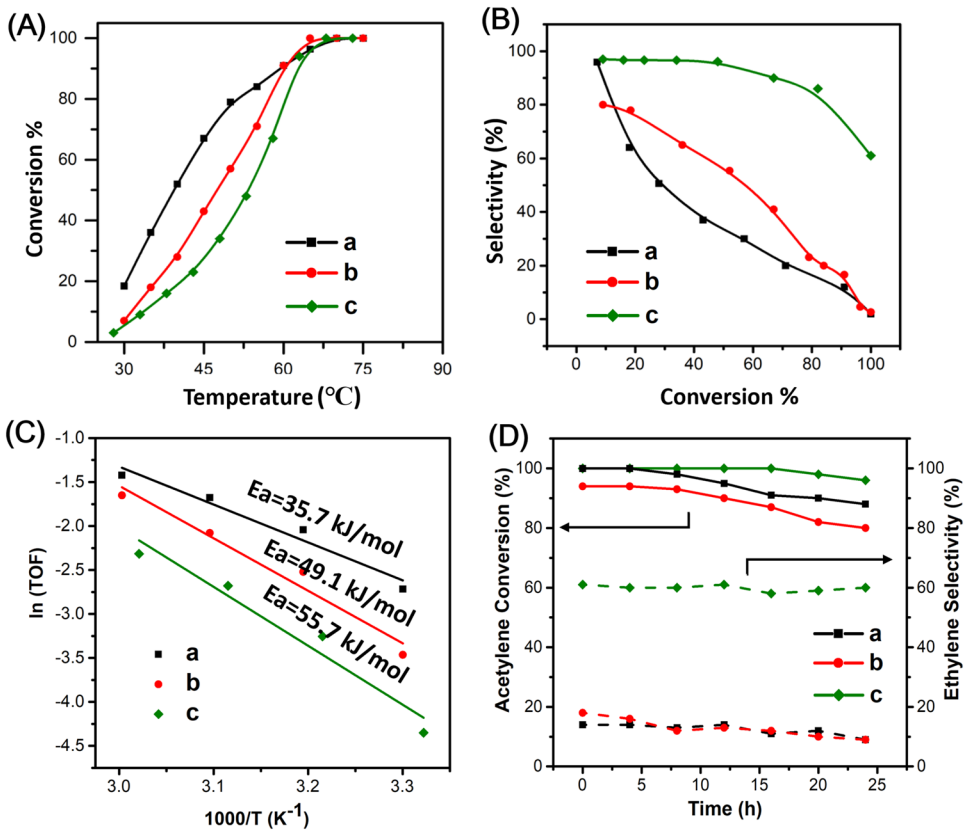

Fig. 4 Plots of **a** acetylene conversion versus temperature, **b** ethene selectivity versus acetylene conversion, **c** Arrhenius plots for acetylene conversion and **d** Stability test over (a) Pd-Cl, (b) Pd-S, and (c) Pd-ac

E_a explains the higher activity on Pd-Cl catalyst than Pd-S and Pd-ac.

The electron-deficient surface is beneficial to the activation of hydrogen, so as to improve the activity. According to the XPS results, the electron density of Pd is in order of Pd-S > Pd-Cl > Pd-ac. Therefore, the Pd-S and Pd-Cl perform higher acetylene conversion than Pd-ac under the same temperature. Additionally, the positive role of chloride ions in promoting the overall catalytic activity can be attributed to the difference dispersion in palladium particles. Pd-Cl catalysts with small Pd particle sizes would have larger interfacial contact areas and thus stronger ability to activate and dissociate H_2 than that of other two catalysts, which contains relatively large palladium particles. In combination with size effect and electron effect, Pd-Cl shows better activity among the three catalysts. To confirm the above speculation, H_2-TPD analysis were conducted (see Fig. 5a). All the catalysts exhibit a desorption peaks at about 90 ℃, corresponding to the decomposition of PdH_x. The peaks at high temperature are attributed to desorption of chemisorbed hydrogen. We can see that the H_2-desorption peak area of Pd-Cl catalyst is larger than Pd-ac and Pd-S, demonstrating that the Pd-Cl has a stronger adsorption ability of hydrogen in agreement with the above analysis.

In the reaction of partial acetylene hydrogenation, selectivity toward ethylene is also a very important parameter. Seen from Fig. 4b, Pd/Al_2O_3 prepared from different Pd precursors displays significant differences in ethylene selectivity. Specifically, when the acetylene conversion ranged from 0 to 80%, the selectivity over Pd-ac catalyst decreased steadily from almost 100% to 83%. Followed by further decreased once the conversion is more than 85% with the reduction of acetylene coverage, and finally maintain at 61% when acetylene fully consumed. However, the selectivity of Pd-Cl and Pd-S declines from the beginning to the end, especially for Pd-S catalyst, selectivity of ethylene is below 80% in the initial stage of the reaction, which is far below Pd-ac catalyst once acetylene was fully consumed. In the reaction of selective acetylene hydrogenation, the selectivity of a catalyst toward ethylene depends on the adsorption strength of ethylene, which is mainly relative to the changes of valence electrons of active Pd metal. The increase of electron density weakened the adsorption of ethylene on the negatively charged Pd sites and hence improved the selectivity. Consequently, C_2H_4-TPD was employed over Pd-Cl, Pd-S and Pd-ac samples in order to investigate the ad- and desorption characteristic of ethylene, and the results are shown in Fig. 5b. The low signal intensity is mainly due to the weak adsorption of ethylene on the Pd surface and the limited signal response of TCD detector. Each catalyst shows one peak ranged from 50 to 100 ℃ assigned to π-bonded ethylene [37]. Compared with Pd-Cl and Pd-S catalyst, the peak

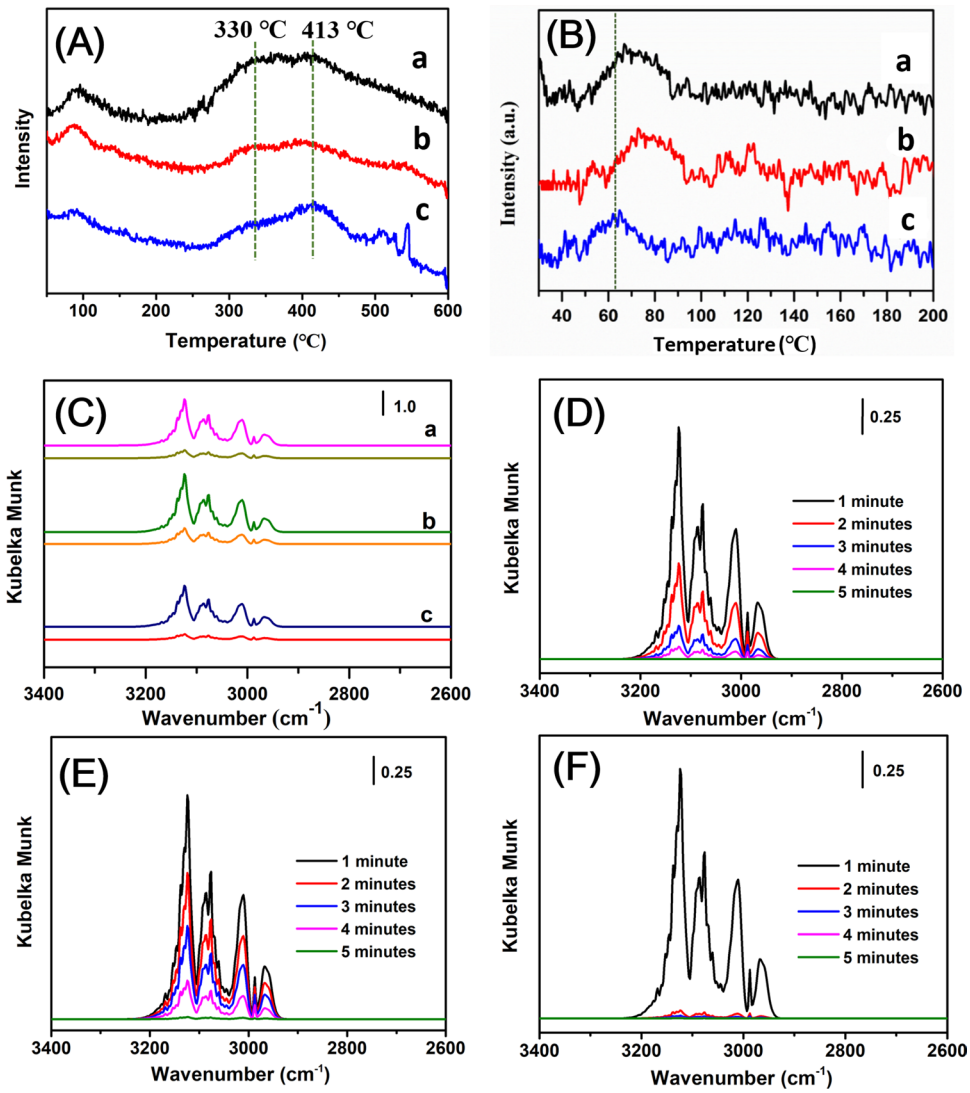

Fig. 5 **a** H_2-TPD, **b** C_2H_4 -TPD and **c** C_2H_4 –IR profiles of adsorption and desorption at room temperature over Pd-Cl (a), Pd-S (b) and Pd-ac (c). C_2H_4 –IR profiles of desorption at 60 ℃ with time for **d** Pd-Cl, **e** Pd-S, and **f** Pd-ac

in Pd-ac sample exhibits at lower temperature by approximately 15 ℃, indicating that desorption of ethylene from the surface of Pd-ac catalyst is easier than other two catalysts.

Due to the low TCD signal, C_2H_4-TPD result is unconvincing, and therefore, in situ IR of C_2H_4 was further employed. As shown in Fig. 5c, it appears the characteristic peak of ethylene [39] at 3122, 3089, 3076, 3008, and 2966 cm^{-1} after treating in ethylene for half hour at room temperature, followed by purging in nitrogen until the intensity stay unchanged. In comparison with Pd-Cl and Pd-S catalysts, the intensity of C_2H_4-IR spectra descended distinctly. Then, the catalysts were further purged by nitrogen flow at 60 ℃. The changes of ethylene adsorption over Pd-Cl, Pd-S, and Pd-ac catalysts were recorded at per minute and shown in Fig. 5d–f. As for Pd-ac catalyst, the adsorption intensity of ethylene decreases obviously with time compared to Pd-S and Pd-Cl catalysts, suggesting the adsorbates are easier to remove on its surface, which is in good agreement with the results obtained from C_2H_4-TPD. According to the H_2-TPD, C_2H_4-TPD and C_2H_4-IR results, the main difference of catalytic performance can be reasonably ascribed to the change of electronic structure instead of geometric configuration, although the existence of Cl and S separates the continuous Pd active sites to a certain extent.

Time-on-stream analysis of all the three Pd/Al_2O_3 catalyst in partial hydrogenation of acetylene was investigated at 70 ℃ with the relative pressure of 0.4 MPa for 24 h on stream as shown in Fig. 4d. The acetylene conversion of Pd-ac catalysts maintains a relative stable state with only 5% decreases of the activity after 24 h and the selectivity of ethylene still remaining 60%. However, both the activity and selectivity of Pd-Cl and Pd-S catalyst decreases significantly. The variation of structure in the reaction process and the reason of inactivation deserve to be studied. Firstly, we characterized the morphology and size of the used nanoparticles by TEM presented in Fig. 6a–c. The average size of Pd nanoparticles

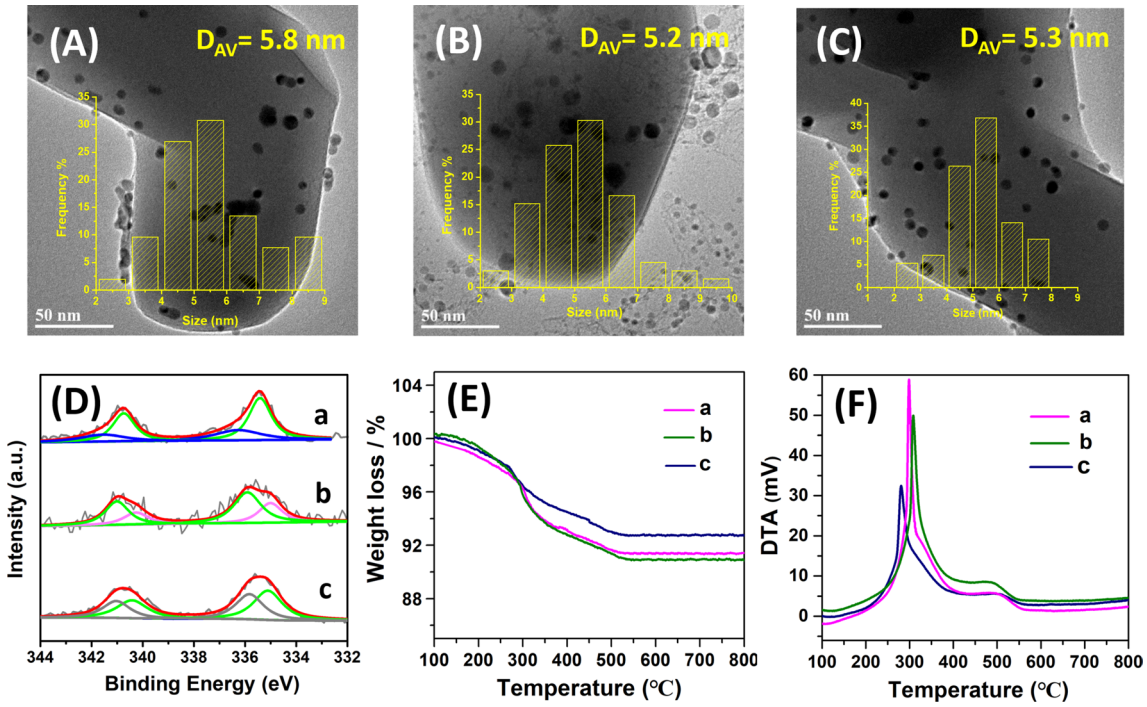

Fig. 6 HRTEM images of used catalysts over Pd-Cl (**a**), Pd-S (**b**), and Pd-ac (**c**). XPS (**d**), TG (**e**) and DTA (**f**) curves of used catalysts over (a) Pd-Cl, (b) Pd-S and (c) Pd-ac

after reaction of three catalysts grew bigger, but the Pd-Cl catalyst showed more obvious agglomeration of Pd particles due to the presence of chlorine usually leading to the sintering of catalysts reported by literature [6, 8].

The electronic structure of used catalysts was further explored by XPS (Fig. 6d). The binding energy of Pd $3d_{2/5}$ for used Pd-Cl catalyst is 335.5 eV, which is similar to the fresh catalyst. Therefore, the inactivation of Pd-Cl catalyst is mainly due to the sintering of Pd nanoparticles. In case of used Pd-ac and Pd-S catalyst, XPS peaks underwent a significance change. For used Pd-ac catalyst, there is no obvious change for $3d_{5/2}$ of Pd^0 (335.2 eV). However, the $3d_{5/2}$ of Pd^{2+}at 336.9 eV was replaced by the peak at 335.8 eV assigned to Pd–C species [40]. According to the literature [41], the formation of Pd–C species is beneficial to the improvement of ethylene selectivity. Therefore, the Pd-ac catalyst performed preferable stability than Pd-Cl and Pd-S. As for the used Pd-S catalyst, the characteristic peaks of Pd^{2+} disappeared, meanwhile a new peak around 335.0 eV appeared which is close to Pd^0 $3d_{5/2}$ of Pd metal. In addition, the $3d_{5/2}$ of Pd^0 peak in fresh Pd-S moved from 336.3 eV to 335.9 eV. These phenomenon may be ascribed to the structure with S insertion into the Pd lattice is unstable and the two elements are segregated in the reaction process. However, the movement to lower binding energy of Pd element, which is conducive to ethylene desorption, fall flat on improvement of ethylene selectivity and stability. As the other possible pathways of C_2H_2 hydrogenation happens, deactivation may be related to coke formation during the reaction process, the composition and content of which influenced by the differences electronic environment of Pd/Al_2O_3. Therefore, we further studied the carbon deposition of three catalysts.

Thermogravimetric-differential thermal analysis was performed over the used catalysts after 24 h continuous reaction. As shown in Fig. 6c, the lowest carbon deposition of 7.2% is measured on Pd-ac catalyst, while the highest value of 9.1% is observed on the Pd-S catalyst. The fresh Pd/Al_2O_3 catalysts (Figure S1) show no weight loss beyond that expected for adsorbed water, so the weight loss of the used catalysts over 100 ℃ is attributed to carbon depositions. As a result, there is a direct relation between the deactivation of the catalysts and the carbon depositions. In the DTA curves, two peaks are observed for each catalyst at around 300 °C and 500 °C, which can be attributed to the combustion of heavy hydrocarbons and fixed coke, respectively [14]. It's worth noting that the intensity of exothermic peak over Pd-ac catalyst in the DTA curve is lower than that of Pd-Cl and Pd-S catalysts. Moreover, the exothermic peak of Pd-S and Pd-Cl catalyst shifts to higher temperature with respect to Pd-ac catalyst. These results suggest higher content of heavy hydrocarbon and coke in Pd-Cl and Pd-S catalysts compared to Pd-ac catalyst, explaining the stability of Pd-ac catalysts.

$PdCl_4^{2-}$, $PdSO_4$, and Pd $(acac)_2$ were used to study the influence of palladium precursor on structural properties of Pd/Al_2O_3 catalyst and the characteristics in selective acetylene hydrogenation. Performance evaluation results show Pd/Al_2O_3 catalyst with Pd $(acac)_2$ as the precursor has better ethylene selectivity and stability in comparison with $PdCl_4^{2-}$ and $PdSO_4$ precursor at the certain conversion. The analysis of structural characterization indicate that the residual Cl still mainly exists in the form of $PdCl_4^{2-}$ complexes and the S residua insets into the Pd crystal lattice, while the C element remains on the catalyst surface as a carbon atom. The different existence forms of precursor residua result in the change for valance state and surface atomic environment of Pd active component. The Pd-ac has higher electron density around Pd sites in comparison with Pd-Cl and Pd-S, which is in favor of desorption of ethylene molecules, and thus performed higher ethylene selectivity. In addition, the Pd-Cl catalyst shows better dispersion than Pd-S and Pd-ac catalysts. Therefore, the Pd-Cl catalyst performed slightly higher activity. Furthermore, the Pd-ac can still maintain a good activity and selectivity after 24 h usage due to the formation of PdC species during reaction process.

4 Conclusion

In summary, we have investigated the effect of the metal precursor by preparing usual Pd/Al_2O_3 catalysts from $PdCl_4^{2-}$, $PdSO_4$, and $Pd(acac)_2$. The existence form and species of precursor residues are very different, so it has important influence on the valence electron structure and dispersion of the catalysts. The Cl residua exists in the form of $PdCl_4^{2-}$ complexes and the S residua insets into the Pd crystal lattice, while the C element remains on the catalyst surface as a carbon atom. The catalysts with different precursor were evaluated in selective hydrogenation of acetylene. The Pd-ac exhibited more satisfying ethylene selectivity than Pd-Cl and Pd-S due to the higher electron density of Pd active sites. In addition, owing to the formation of PdC species during long time reaction, the Pd-ac is more stable than the other two catalysts. According to the above results, the $Pd(acac)_2$ is a promising precursor for the industrial application catalysts.

Supplementary Information The online version contains supplementary material available at https://doi.org/10.1007/s10562-021-03620-w.

Acknowledgements This work was supported by the National Key Research and Development Program of China (No. 2017YFE0301502), the National Natural Science Foundations of China (22078007, 21627813, 21521005, 21908002), the Fundamental Research Funds for the Central Universities (XK1802-6, JD2004, buctrc201921), project funded by China Postdoctoral Science Foundation (2019M660416).

Declarations

Conflict of interest The authors declares that they have no conflict of interest.

References

1. Kinnunen NM, Suvanto M, Moreno MA, Savimäki A, Kallinen K, Kinnunen TJJ, Pakkanen TA (2009) Methane oxidation on alumina supported palladium catalysts: effect of Pd precursor and solvent. Appl Catal A 370:78–87
2. Marques R, Mazri L, Da Costa S, Delacroix F, Djéga-Mariadassou G, Da Costa P (2008) Selective reduction of NOx by hydrogen and methane in natural gas stationary sources over alumina-supported Pd Co and Co/Pd catalysts. Catal Today 137:179–184
3. Sterchele S, Biasi P, Centomo P, Shchukarev A, Kordás K, Rautio A-R, Mikkola J-P, Salmi T, Canton P, Zecca M (2016) Influence of metal precursors and reduction protocols on the chloride-free preparation of catalysts for the direct synthesis of hydrogen peroxide without selectivity enhancers. ChemCatChem 8:1564–1574
4. Mahata N, Vishwanathan V (2000) Influence of palladium precursors on structural properties and phenol hydrogenation characteristics of supported palladium catalysts. J Catal 196:262–270
5. Lin S, Yang X, Yang L, Zhou R (2015) Three-way catalytic performance of $Pd/Ce_{0.6}7Zr_{0.33}O_2$–Al_2O_3 catalysts: role of the different Pd precursors. Appl Surf Sci 327:335–343
6. Xie Y-H, Li B, Weng W-Z, Zheng Y-P, Zhu K-T, Zhang N-W, Huang C-J, Wan H-L (2015) Mechanistic aspects of formation of sintering-resistant palladium nanoparticles over SiO_2 prepared using $Pd(acac)_2$ as precursor. Appl Catal A 504:179–186
7. Selishchev DS, Kolobov NS, Bukhtiyarov AV, Gerasimov EY, Gubanov AI, Kozlov DV (2018) Deposition of Pd nanoparticles on TiO_2 using a $Pd(acac)_2$ precursor for photocatalytic oxidation of CO under UV-LED irradiation. Appl Catal B 235:214–224
8. Li B, Li H, Weng W-Z, Zhang Q, Huang C-J, Wan H-L (2013) Synthesis gas production from partial oxidation of methane over highly dispersed Pd/SiO_2 catalyst. Fuel 103:1032–1038
9. Panpranot J, Tangjitwattakorn O, Praserthdam P, Goodwin JG (2005) Effects of Pd precursors on the catalytic activity and deactivation of silica-supported Pd catalysts in liquid phase hydrogenation. Appl Catal A 292:322–327
10. Marceau E, Lauron-Pernot H, Che M (2001) Influence of the metallic precursor and of the catalytic reaction on the activity and evolution of $Pt(Cl)/\delta$-Al_2O_3 catalysts in the total oxidation of methane. J Catal 197:394–405
11. McCue AJ, Anderson JA (2015) Recent advances in selective acetylene hydrogenation using palladium containing catalysts. Front Chem Sci Eng 9:142–153
12. He Y, Liu Y, Yang P, Du Y, Feng J, Cao X, Yang J, Li D (2015) Fabrication of a PdAg mesocrystal catalyst for the partial hydrogenation of acetylene. J Catal 330:61–70
13. Liu Y, Zhao J, He Y, Feng J, Wu T, Li D (2017) Highly efficient PdAg catalyst using a reducible Mg-Ti mixed oxide for selective hydrogenation of acetylene: role of acidic and basic sites. J Catal 348:135–145
14. Ma R, He Y, Feng J, Hu Z-Y, Van Tendeloo G, Li D (2019) A facile synthesis of Ag@PdAg core-shell architecture for efficient purification of ethene feedstock. J Catal 369:440–449
15. McCue AJ, McRitchie CJ, Shepherd AM, Anderson JA (2014) Cu/Al_2O_3 catalysts modified with Pd for selective acetylene hydrogenation. J Catal 319:127–135

16. Liu Y, He Y, Zhou D, Feng J, Li D (2016) Catalytic performance of Pd-promoted Cu hydrotalcite-derived catalysts in partial hydrogenation of acetylene: effect of Pd–Cu alloy formation. Catal Sci Technol 6:3027–3037
17. Pei G, Liu X, Chai M, Wang A, Zhang T (2017) Isolation of Pd atoms by Cu for semi-hydrogenation of acetylene: effects of Cu loading. Chin J Catal 38:1540–1548
18. Zhou H, Yang X, Li L, Liu X, Huang Y, Pan X, Wang A, Li J, Zhang T (2016) PdZn intermetallic Nanostructure with Pd–Zn–Pd ensembles for highly active and chemoselective semi-hydrogenation of acetylene. ACS Catal 6:1054–1061
19. Hu M, Zhao S, Liu S, Chen C, Chen W, Zhu W, Liang C, Cheong WC, Wang Y, Yu Y, Peng Q, Zhou K, Li J, Li Y (2018) MOF-confined sub-2 nm atomically ordered intermetallic PdZn nanoparticles as high-performance catalysts for selective hydrogenation of acetylene. Adv Mater. https://doi.org/10.1002/adma.201801878
20. Marc Armbruster KK, Malte B, Detre T, Yuri G, Robert S (2010) Pd-Ga intermetallic compounds as highly selective semihydrogenation catalysts. J Am Chem Soc 132:14745–14747
21. He Y, Liang L, Liu Y, Feng J, Ma C, Li D (2014) Partial hydrogenation of acetylene using highly stable dispersed bimetallic Pd–Ga/MgO–Al_2O_3 catalyst. J Catal 309:166–173
22. Ma R, Yang T, Sun J, He Y, Feng J, Miller JT, Li D (2019) Nanoscale surface engineering of $PdCo/Al_2O_3$ catalyst via segregation for efficient purification of ethene feedstock. Chem Eng Sci 210:115216
23. He Y, Fan J, Feng J, Luo C, Yang P, Li D (2015) Pd nanoparticles on hydrotalcite as an efficient catalyst for partial hydrogenation of acetylene: effect of support acidic and basic properties. J Catal 331:118–127
24. Mears DE (1971) Tests for transport limitations in experimental catalytic reactors. Ind Eng Chem Process Des Dev 10:541–547
25. Oyama S, Zhang X, Lu J, Gu Y, Fujitani T (2008) Epoxidation of propylene with H_2 and O_2 in the explosive regime in a packed-bed catalytic membrane reactor. J Catal 257:1–4
26. Bachiller-Baeza B, Iglesias-Juez A, Castillejos-López E, Guerrero-Ruiz A, Michiel MD, Fernández-García M, Rodríguez-Ramos I (2015) Detecting the genesis of a high-performance carbon-supported Pd sulfide nanophase and its evolution in the hydrogenation of butadiene. ACS Catal 5:5235–5241
27. Bozon-Verduraz F, Omar A, Escard J, Pontvianne B (1978) Chemical State And Reactivity I. Characterization by XPS and w-visible of supported palladium spectroscopy. J Catal 53:126–134
28. Elding LI, Olsson LF (1978) Electronic absorption spectra of square-planar chloro-aqua and bromo-aqua complexes of palladium(II) and platinum(II). J Phys Chem 82:69–74
29. Ferreira AP, Henriques C, Ribeiro MF, Ribeiro FR (2005) SCR of NO with methane over Co-HBEA and PdCo-HBEA catalysts. The promoting effect of steaming over bimetallic catalyst. Catal Today 107–108:181–191
30. Padmasri AH, Venugopal A, Krishnamurthy J, Rama Rao KS, Kanta Rao P (2002) Novel calcined Mg-Cr hydrotalcite supported Pd catalysts for the hydrogenolysis of CCl_2F_2. J Mol Catal A: Chem 181:73–80
31. Liu Y, McCue AJ, Miao C, Feng J, Li D, Anderson JA (2018) Palladium phosphide nanoparticles as highly selective catalysts for the selective hydrogenation of acetylene. J Catal 364:406–414
32. Santiago G-Q, Fernando C-L, Keane MA (2008) Effect of metal dispersion on the liquid-phase hydrodechlorination of 2,4-dichlorophenol over Pd/Al_2O_3. Ind Eng Chem Res 47:6841–6853
33. Seah DB (1995) Practical surface analysis by auger and X-Ray photoelectron spectroscopy. Anal Chim Acta 306:2–3
34. Álvarez-Montero MA, Gómez-Sainero LM, Martín-Martínez M, Heras F, Rodriguez JJ (2010) Hydrodechlorination of chloromethanes with Pd on activated carbon catalysts for the treatment of residual gas streams. Appl Catal B 96:148–156
35. Lee WZ (2008) Particle size effects in Pd-Catalyzed electrooxidation of formic acid. J Phys Chem C 112:3789–3793
36. Liu Y, McCue AJ, Feng J, Guan S, Li D, Anderson JA (2018) Evolution of palladium sulfide phases during thermal treatments and consequences for acetylene hydrogenation. J Catal 364:204–215
37. Cao Y, Sui Z, Zhu Y, Zhou X, Chen D (2017) Selective hydrogenation of acetylene over $Pd\text{-}In/Al_2O_3$ catalyst: promotional effect of indium and composition-dependent performance. ACS Catal 7:7835–7846
38. Lear T, Marshall R, Lopez-Sanchez JA, Jackson SD, Klapotke TM, Baumer M, Rupprechter G, Freund HJ, Lennon D (2005) The application of infrared spectroscopy to probe the surface morphology of alumina-supported palladium catalysts. J Chem Phys 123:174706
39. Liu Y, McCue AJ, Yang P, He Y, Zheng L, Cao X, Man Y, Feng J, Anderson JA, Li D (2019) Support morphology-dependent alloying behaviour and interfacial effects of bimetallic $Ni\text{-}Cu/CeO_2$ catalysts. Chem Sci 10:3556–3566
40. Teschner D, Borsodi J, Wootsch A, Revay Z, Havecker M, Knop-Gericke A, Jackson SD, Schlogl R (2008) The roles of subsurface carbon and hydrogen in palladium-catalyzed alkyne hydrogenation. Science 320:86–89
41. Liu Y, Fu F, McCue A, Jones W, Rao D, Feng J, He Y, Li D (2020) Adsorbate-induced structural evolution of Pd catalyst for selective hydrogenation of acetylene. ACS Catal 10:15048–15059

Authors and Affiliations

Tianxing Yang[1] · Min Zhao[1] · Xue Wang[1] · Rui Ma[2] · Yanan Liu[1,3] · Yufei He[1,3] · Dianqing Li[1,3]

[1] State Key Laboratory of Chemical Resource Engineering, Beijing University of Chemical Technology, Box 98, 15 Bei San Huan East Road, Beijing 100029, China

[2] Chemistry and Chemical Engineering Guangdong Laboratory, Shantou 515031, China

[3] Beijing Engineering Center for Hierarchical Catalysts, Beijing University of Chemical Technology, Beijing 100029, China